

Experimental study of the level structure in ^{90}Nb and systematics of level structure characteristics near $A = 90$

Yi-Heng Wu ^{1,2}, Jing-Bin Lu,^{1,*} Zhen Ren,¹ Guan-Jian Fu,³ Cheng-Qian Li,¹ Pei-Yao Yang ¹, Yan Hao,¹ Tian-Jiao Gao,¹ Li-Hua Zhu,⁴ Xing-Zhu Cui,⁵ Xiao-Guang Wu,⁶ and Chuang-Ye He⁶

¹College of Physics, Jilin University, Changchun 130012, China

²School of Electronic Engineering and Intelligent Manufacturing, Anqing Normal University, Anqing 246133, China

³School of Physics Science and Engineering, Tongji University, Shanghai 200092, China

⁴School of Physics, Beihang University, Beijing 100191, China

⁵Institute of High Energy Physics, Chinese Academy of Sciences, Beijing 100049, China

⁶China Institute of Atomic Energy, Beijing 102413, China



(Received 3 August 2023; accepted 26 January 2024; published 26 February 2024)

In beam γ -ray spectroscopic investigations of the ^{90}Nb nucleus have been explored by employing the $^{76}\text{Ge}(^{19}\text{F}, 5n)^{90}\text{Nb}$ reaction. Twenty-eight new transitions belonging to ^{90}Nb have been identified and placed in the proposed level scheme through the analysis of γ - γ coincidence spectra. Shell model calculations have been performed in the restricted $\pi(p_{3/2}, f_{5/2}, p_{1/2}, g_{9/2}) \otimes \nu(p_{1/2}, g_{9/2}, d_{5/2}, g_{7/2})$ configuration space, and compared to the new level scheme. According to the calculations, the newly observed 2614.6 keV γ ray depopulating the (15_3^+) level at 4421.2 keV is explicated as the breakup of the $N = 50$ neutron closed shell, while the γ ray with 2774.0 keV feeding the (13_1^-) level at 2812.9 keV is interpreted as protons excitation across the $Z = 38$ subshell.

DOI: [10.1103/PhysRevC.109.024326](https://doi.org/10.1103/PhysRevC.109.024326)

I. INTRODUCTION

The level schemes of nuclei near the neutron number $N = 50$ and the proton number $Z = 40$ have been extensively studied both experimentally and theoretically. These studies can provide valuable and abundant information to ameliorate the effective interaction within a shell-model framework, especially in the shell-model Hamiltonian for interactions of protons and neutrons in the $p_{3/2}$, $f_{5/2}$, $p_{1/2}$, and $g_{9/2}$ shells [1–10]. It is common knowledge that excitations of the core are indispensable to elucidate the characteristics of the level structures in nuclei with magic numbers of protons or neutrons. The high-spin levels of ^{86}Kr [11], ^{91}Nb [6], ^{93}Tc [12], ^{94}Ru [13], and ^{95}Rh [14] nuclei with $N = 50$ cannot be fully explicated by the pure proton configurations, but explained by breaking the closed neutron shell and the promotion of one neutron across the shell gap to the $d_{5/2}$ orbital.

Adjacent to the $N = 50$ shell closure, the spherical shell model has been proven to be effective for understanding the level structures in $N = 47$ isotones ^{88}Nb [15], ^{89}Mo [16], ^{90}Tc [17], and ^{91}Ru [18]. In $N = 46$ isotones ^{88}Mo [19], ^{89}Tc [20], ^{90}Ru [21], ^{86}Zr [22], and ^{87}Nb [23], several enhanced $B(E2)$ values are observed, which manifest the onset of collectivity. In these nuclei, the abundance of protons in the $g_{9/2}$ orbit or neutron holes in the $g_{9/2}$ orbits relative to the ^{88}Sr core can provide high angular momenta, without the need for additional single-particle orbits or collective core excitations. Protons core excitations from the $(f_{5/2}, p_{3/2}, p_{1/2})$

orbits and/or neutrons excitations of the $g_{9/2}$ orbit across the $N = 50$ shell play pivotal roles in illustrating the gap structure in $N = 49$ isotones [24–28] and the extremely high excitation energies in some $N = 48$ isotones [10,29,30].

The present work is to continue our systematic studies of the Nb isotopes [6–8] and extend the investigations of $N = 49$ isotones by focusing on the high spin levels in ^{90}Nb . Prior to this work, the low-lying and intermediate levels in ^{90}Nb were populated by the β decay of 5.7 h ^{90}Mo [31] reaction, $^{90}\text{Zr}(p, n\gamma)^{90}\text{Nb}$ reaction [32], and $^{89}\text{Y}(\alpha, 3n\gamma)^{90}\text{Nb}$ reaction [33]. The high spin levels in ^{90}Nb were studied via $^{63}\text{Cu}(^{31}\text{P}, 3p1n)^{90}\text{Nb}$ [34] and $^{76}\text{Ge}(^{19}\text{F}, 5n)^{90}\text{Nb}$ reactions [35]. The incentive of this work is to expand the level scheme of ^{90}Nb to the higher spin levels and excitation energies, which are ascribed to the excitation of nucleons over the $Z = 38$ subshell and $N = 50$ shell closure. Special interest in ^{90}Nb is primarily due to the fact that the ^{90}Nb nucleus, with $Z = 41$ and $N = 49$, allows both the proton and the neutron hole to occupy the $g_{9/2}$ orbital, resulting in the information of multiplets states. Thus, a more comprehensive understanding of the excitation energies for the different members of these multiplets can provide insights into the residual nucleon-nucleon interaction.

II. EXPERIMENTS AND RESULTS

The $^{76}\text{Ge}(^{19}\text{F}, 5n\gamma)^{90}\text{Nb}$ experiment was performed at the China Institute of Atomic Energy in Beijing using an 80 MeV ^{19}F beam. A 2.2 mg/cm² target of ^{76}Ge (enrichment 96%) backed with 10 mg/cm² Yb foil was used. Before conducting the experiment, the detectors were calibrated for energy and efficiency using standard sources of ^{60}Co , ^{133}Ba , and ^{152}Eu ,

*ljb@jlu.edu.cn

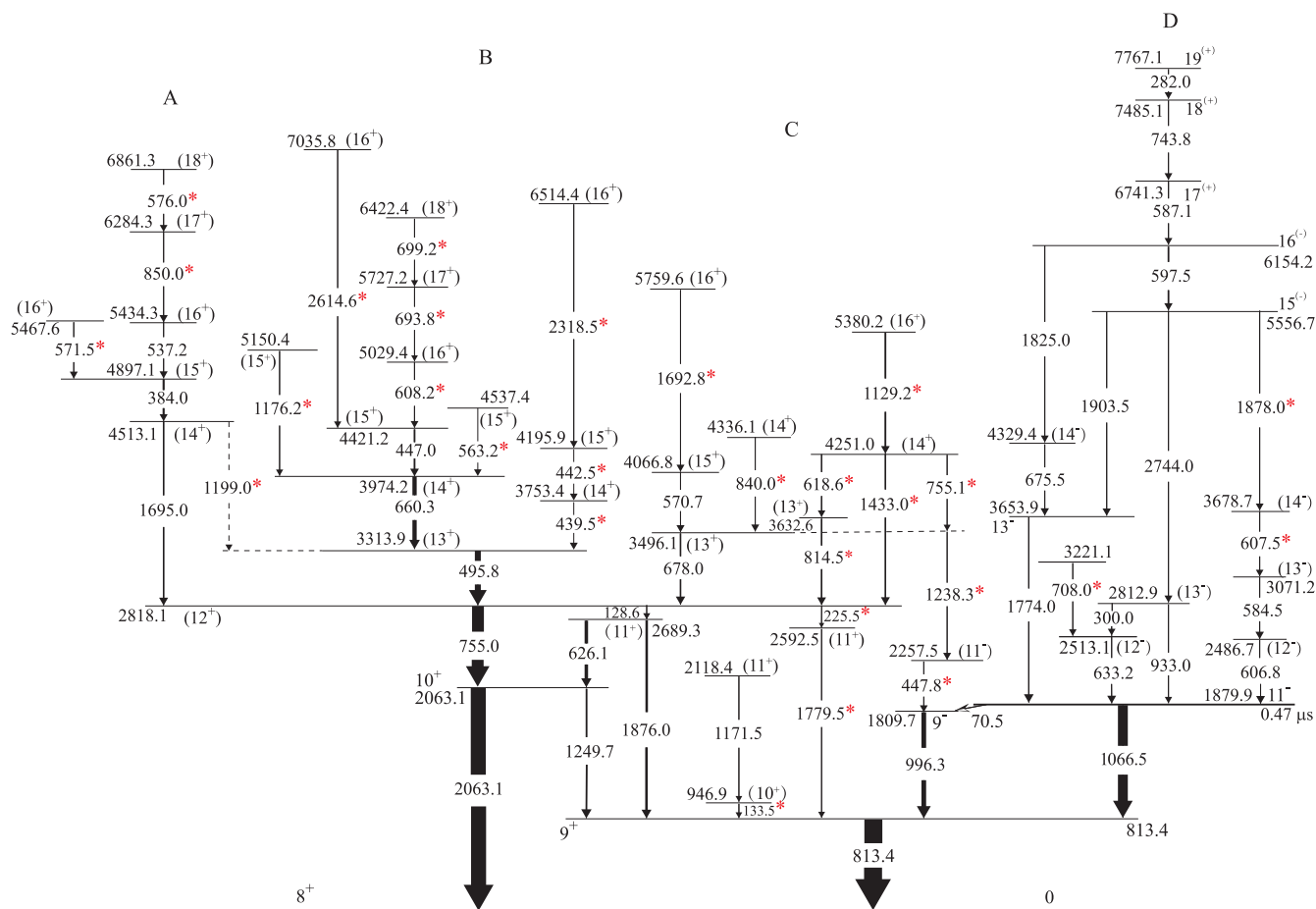


FIG. 1. Proposed level scheme for ^{90}Nb originated from the present and previous work [34,35]. New γ rays are marked with red asterisks. The level and γ transition energies are given in keV. Arrow width stands for the relative γ ray intensity. Spin and parity assignments for levels are tentative.

which covered an energy region from 39.52 keV to 1408.0 keV. In the data processing, more precise energy calibrations were done using characteristic γ rays emitted by the residual nuclei. In order to extract the calibration coefficients, the entire energy range was split into the low and high subdivisions. For the low energy range, the 184.9, 399.0, 421.6, 755.0, 819.2, and 1023.6 keV γ rays were selected, and the 819.2, 1023.6, 1249.7, 1658.1, 2055.0, and 2290.4 keV γ rays were selected for the high energy region (these γ rays stem from ^{87}Y , ^{90}Zr , ^{90}Nb , and ^{91}Nb nuclei).

About a total of 110×10^6 γ - γ coincidence events were gathered and arranged into a two-dimensional symmetrized $E\gamma$ - $E\gamma$ coincidence matrix. An angle dependent matrix between the detectors at 132° (48°) and at 90° was also created and employed to analyze the directional correlation of oriented states (DCO) ratio [29,30]. In the present geometry, R_{DCO} is obtained using the expression

$$R_{\text{DCO}} = \frac{I_{(\gamma_1)} \text{ at } 132^\circ (48^\circ) \text{ gated by } \gamma_2 \text{ at } 90^\circ}{I_{(\gamma_1)} \text{ at } 90^\circ \text{ gated by } \gamma_2 \text{ at } 132^\circ (48^\circ)}.$$

Here, $I_{(\gamma_1)}$ represents the intensity of γ_1 measured in the spectrum gated by γ_2 which coincides with γ_1 . In our array geometry, the R_{DCO} values for a dipole transition extracted from the gating on a quadrupole (dipole) transition are about 0.6

(1.0), whereas for a quadrupole transition extracted from the gating on a quadrupole (dipole) transition is about 1.0 (2.0). The disadvantage of this approach is that it is hard to achieve any possible $M1$, $E2$ admixtures. Therefore, spin and parity are tentatively assigned on the basis of the reported data, the DCO values from the present measurements, and shell model calculations. The new level scheme for ^{90}Nb , as depicted in Fig. 1, is grouped into four parts and labeled with sequential letters (A, B, C, and D) to aid in discussion. The placements of new γ rays in the level scheme were appointed by means of their coincidence relationships, energy summings, and intensity balances. Properties of the levels and transitions deduced from the present measurements are tabulated in Table I, and several coincidence spectra are exhibited in Figs. 2, 3, and 4.

In part A of Fig. 1, a sequence $576.0 \rightarrow 850.0 \rightarrow 537.2 \rightarrow 384.0 \rightarrow 1695.0$ keV, is placed on top of the (12_1^+) level at 2818.1 keV. The ordering of each transition is placed according to the coincidence relations and relative intensities. The sum of gated spectra of the 755.0 and 495.8 keV transitions is shown in Fig. 2. As illustrated in Fig. 2, the new transitions with energies of 576.0 and 850.0 keV are identified. To support the sequence of transitions assigned to ^{90}Nb , we present the coincidence spectrum gated on the 1695.0 keV transition in Fig. 3, and the sum of the 576.0 and 537.2 keV

TABLE I. γ ray energy (E_γ), DCO value, relative intensity (I_γ), initial and final spins (J_i) and (J_f), initial and final excitation energies (E_i) and (E_f) in ^{90}Nb nucleus.

E_γ^a (keV)	I_γ^b	R_{DCO}		E_i^π (keV)	E_f^π (keV)	J_i^π (\hbar)	J_f^π (\hbar)
		($\Delta I = 1$ gate)	($\Delta I = 2$ gate)				
70.5				1879.9	1809.7	11_1^-	9^-
128.6				2818.1	2689.3	(12_3^+)	(11_3^+)
133.5	2.67 (70)			946.9	813.4	(10_1^+)	9^+
225.5				2818.1	2592.5	(12_1^+)	(11_2^+)
282.0	2.69 (13)			7767.1	7485.1	$19^{(+)}$	$18_3^{(+)}$
300.0	3.31 (32)			2812.9	2513.1	(13_1^-)	(12_2^-)
384.0	6.31 (71)		0.61 (8) ^c	4897.1	4513.1	(15_3^+)	(14_3^+)
439.5	4.46 (20)			3753.4	3313.9	(14_1^+)	(13_1^+)
442.5	3.60 (20)			4195.9	3753.4	(15_2^+)	(14_1^+)
447.0	9.81 (41)		0.54 (6) ^c	4421.2	3974.2	(15_3^+)	(14_2^+)
447.8				2257.5	1809.7	(11_2^-)	9^-
495.8	33.2 (20)		0.69 (4) ^c	3313.9	2818.1	(13_1^+)	(12_1^+)
537.2	5.07 (80)		0.63 (7) ^c	5434.3	4897.1	(16_3^+)	(15_5^+)
563.2	5.35 (38)	1.05 (7) ^d		4537.4	3974.2	(15_4^+)	(14_2^+)
570.7	4.79 (33)	1.9 (3) ^d		4066.8	3496.1	(15_1^+)	(13_2^+)
571.5				5467.6	4897.1	(16_4^+)	(15_5^+)
576.0	3.61 (34)		0.58 (8) ^c	6861.3	6284.3	(18_3^+)	(17_2^+)
584.5	5.3 (11)	0.9 (2) ^d		3071.2	2486.7	(13_2^-)	(12_1^-)
587.1	6.26 (38)	1.0 (2) ^d		6741.3	6154.2	$17_3^{(+)}$	$16^{(-)}$
597.5	9.37 (80)	1.2 (2) ^d		6154.2	5556.7	$16^{(-)}$	$15^{(-)}$
606.8				2486.7	1879.9	(12_1^-)	11_1^-
607.5	4.26 (47)			3678.7	3071.2	(14_1^-)	(13_2^-)
608.2	6.25 (49)	1.1 (1) ^d		5029.4	4421.2	(16_1^+)	(15_3^+)
618.6	7.08 (92)		0.6 (1) ^c	4251.0	3632.6	(14_3^+)	(13_3^+)
626.1	19.3 (37)	0.9 (1) ^d		2689.3	2063.1	(11_3^+)	10_2^+
633.2	5.00 (50)			2513.1	1879.9	(12_2^-)	11_1^-
660.3	23.79 (94)		0.6 (1) ^c	3974.2	3313.9	(14_2^+)	(13_1^+)
675.5	5.25 (61)	0.7 (1) ^d		4329.4	3653.9	(14_2^-)	13_3^-
678.0	8.87 (35)		0.6 (1) ^c	3496.1	2818.1	(13_2^+)	(12_1^+)
693.8	4.72 (36)	1.0 (2) ^d		5727.2	5029.4	(17_1^+)	(16_1^+)
699.2	4.49 (7)		0.58 (8) ^c	6422.4	5727.2	(18_1^+)	(17_1^+)
708.0	3.53 (40)			3221.1	2513.1	(12_1^-)	(12_2^-)
743.8	3.15 (47)	0.8 (1) ^d		7485.1	6741.3	$18_3^{(+)}$	$17_3^{(+)}$
755.0	66.4 (63)	1.6 (1) ^d		2818.1	2063.1	(12_1^+)	10_2^+
755.1	3.33 (36)		0.5 (2) ^c	4251.0	3496.1	(14_3^+)	(13_2^+)
813.4	100	0.90 (9) ^d		813.4	0	9^+	8^+
814.5	8.3 (12)	0.8 (1) ^d		3632.6	2818.1	(13_3^+)	(12_1^+)
840.0	3.75 (34)	1.1 (3) ^d		4336.1	3496.1	(14_4^+)	(13_2^+)
850.0	4.68 (45)		0.51 (7) ^c	6284.3	3931.3	(17_2^+)	(16_3^+)
933.0	3.43 (44)			2812.9	1879.9	(13_1^-)	11_1^-
996.3	26.7 (22)	1.6 (1) ^d		1809.7	813.4	9^-	9^+
1066.5	56.68 (36)	1.7 (1) ^d		1879.9	813.4	11_1^-	9^+
1129.2	9.79 (84)			5380.2	4251.0	(16_2^+)	(14_3^+)
1171.5	2.17 (71)			2118.4	946.9	(11_1^+)	(10_1^+)
1176.2	4.52 (41)	1.0 (2) ^d		5150.4	3974.2	(15_6^+)	(14_2^+)
1199.0				4513.1	3313.9	(14_5^+)	(13_1^+)
1238.3	5.90 (60)		1.3 (2) ^c	3496.1	2257.5	(13_2^+)	(11_2^-)
1249.7	9.71 (78)	1.2 (2) ^d		2063.1	813.4	10_2^+	9^+
1433.0	8.40 (70)		1.0 (2) ^c	4251.0	2818.1	(14_3^+)	(12_1^+)
1692.8	4.98 (44)			5759.6	4066.8	(16_5^+)	(15_1^+)
1695.0	8.4 (1)			4513.1	2818.1	(14_5^+)	(12_1^+)
1774.0	6.8 (12)	1.5 (2) ^d		3653.9	1879.9	13_3^-	11_1^-
1779.5	3.89 (10)			2592.5	813.4	(11_2^-)	9^+
1825.0				6154.2	4329.4	$16^{(-)}$	(14_2^-)
1876.0	13.9 (13)	2.07 (31) ^d		2689.3	813.4	(11_3^+)	9^+

TABLE I. (Continued.)

E_γ^a (keV)	I_γ^b	R_{DCO}		E_i^π (keV)	E_f^π (keV)	J_i^π (\hbar)	J_f^π (\hbar)
		($\Delta I = 1$ gate)	($\Delta I = 2$ gate)				
1878.0				5556.7	3678.7	15^{-}	(14_1^-)
1903.5	5.18 (72)		0.98 (18) ^c	5556.7	3653.9	15^{-}	13_3^-
2063.1	83.6 (86)		0.88 (6) ^c	2063.1	0	10_2^+	8^+
2318.5	2.39 (23)			6514.4	4195.9	(16_6^+)	(15_2^+)
2614.6	2.57 (21)			7035.8	4421.2	(16_7^+)	(15_3^+)
2744.0				5556.7	2812.9	15^{-}	(13_1^-)

^aThe uncertainty in strong γ -ray energies ($I_\gamma > 10$) is about 0.4 keV and about 0.7 keV for weak transitions ($I_\gamma < 10$).

^bIntensities are corrected for detector efficiency and normalized to 100 for the 813.4 keV γ ray.

^cGated transitions are of $\Delta I = 2$ nature.

^dGated transitions are of $\Delta I = 1$ nature.

transitions in Fig. 4. From the spectrum gated on the 1695.0 keV transition, as shown in Fig. 3, two new transitions with 576.0 and 850.0 keV as well as the known transitions with 384.0, 537.2, 755.0, 813.4, 626.1, 1249.7, and 2063.1 keV can be identified. In addition, the transitions with 576.0, 850.0, 384.0, 537.2, 755.0, 813.4, 626.1, 1249.7, 1695.0, and 2063.1 keV are clearly seen in the spectrum gated on the sum of the 576.0 and 537.2 keV transitions (shown in Fig. 4). A new transition with 571.5 keV is observed in the present work, which is coincidence with the 384.0, 495.8, and 1695.0 keV transitions, etc. However, it is not in coincidence with the 537.2, 850.0, and 576.0 keV transitions. Therefore, the 571.5 keV γ ray is aligned parallel to the 537.2 keV transition. The 571.5 and 1695.0 keV transitions have too low intensities to extract DCO values. We tentatively propose the 1695.0 keV

transition as $\Delta I = 2$ character, which is consistent with our shell model calculation.

In part B, nine new transitions with 439.5, 442.5, 563.2, 608.2, 693.8, 699.2, 1176.2, 2318.5, and 2614.6 keV are built upon the (13_1^+) state at 3313.9 keV. Based on the calculations, the 2318.5 and 2614.6 keV transitions are tentatively suggested as $\Delta I = 1$ character. A new cascade of transitions with energies of 608.2, 693.8, and 699.2 keV is located above the (15_3^+) level at 4421.2 keV.

As for part C, above the (12_1^+) state at 2818.1 keV, six new transitions with energies of 618.6, 755.1, 814.5, 1129.2, 1433.0, and 1692.8 keV are added to the level scheme. The DCO values manifest that the 618.6, 755.1, and 814.5 keV γ rays are of $\Delta I = 1$ character and the 1433.0 keV γ ray is of $\Delta I = 2$ character. A new 840.0 keV transition is observed

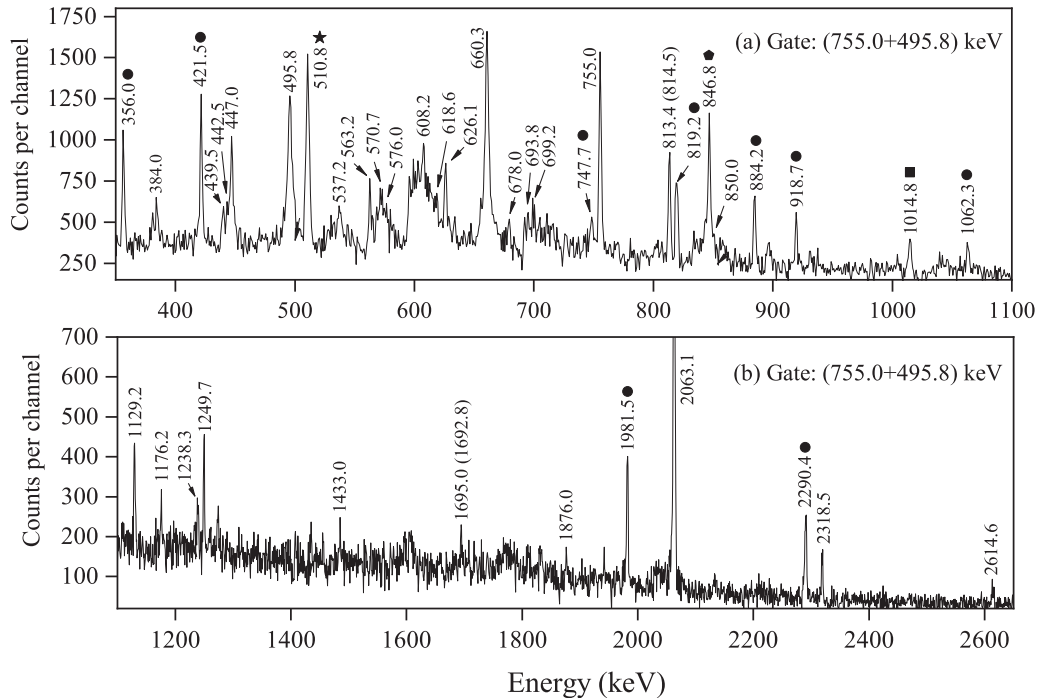


FIG. 2. γ - γ coincidence spectrum with the sum gated on the 755.0 and 495.8 keV transitions. The numbers displayed in the spectra are the peak energies in keV. The peaks marked with circles, a square, a pentagon, and a star originated from the reactions $^{76}\text{Ge} (^{19}\text{F}, 4n) ^{91}\text{Nb}$, $^{27}\text{Al}(n, n')$, Coulomb excitation of ^{56}Fe , and electron positron annihilation, respectively.

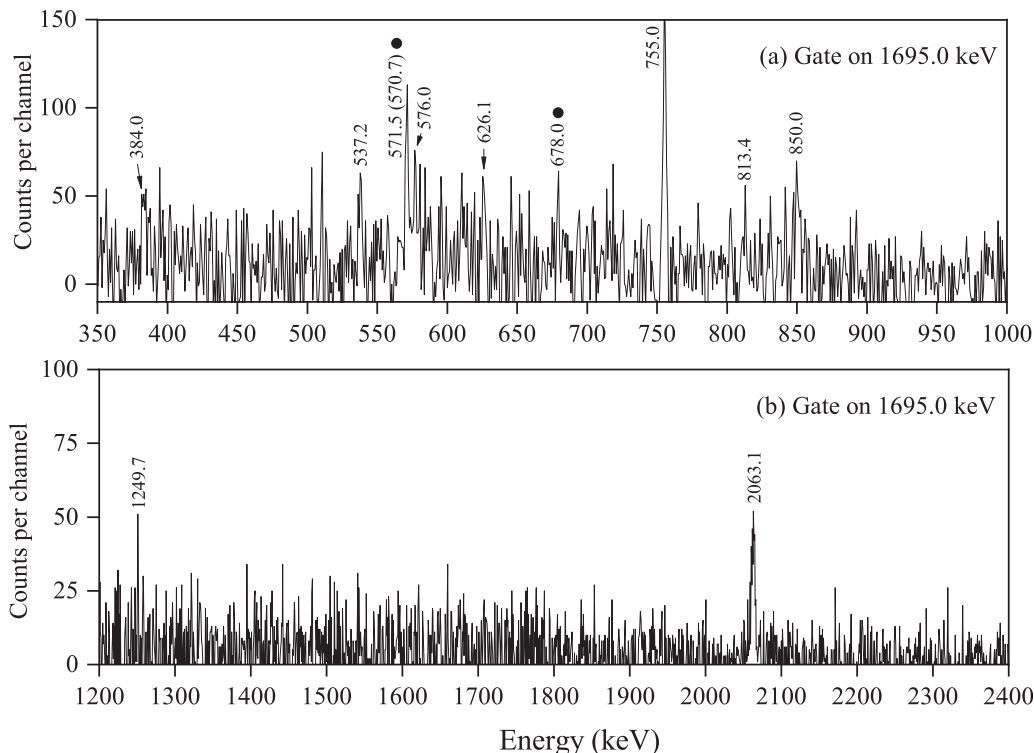


FIG. 3. γ - γ coincidence spectra gated on the 1695.0 keV γ ray. The numbers displayed in the spectra are the peak energies in keV. The peaks with black circles are contaminated by the 1692.8 keV γ ray.

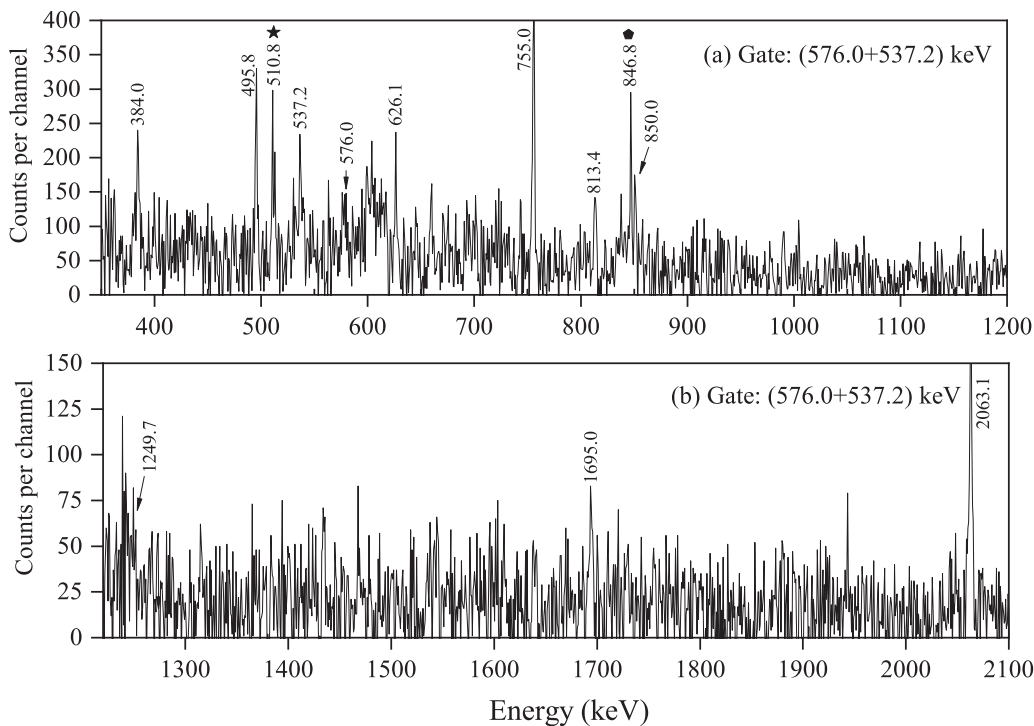


FIG. 4. γ - γ coincidence spectrum with the sum gated on the 537.2 and 576.0 keV transitions. The numbers displayed in the spectra are the peak energies in keV. The peaks with a pentagon and a star originated from the Coulomb excitation of ^{56}Fe and electron positron annihilation, respectively.

the 1695.0 keV γ ray, rather than the 1692.8 keV γ ray. To further illustrate our assignment, Fig. 5 shows a comparison of the coincidence spectra gated by the 384.0 and 678.0 keV γ transitions focused on the region near 1694.0 keV. From Fig. 5, the 1692.8 keV transition is observed in the spectrum on the 678.0 keV γ ray, while the 1695.0 keV transition is observed in the spectrum on the 384.0 keV γ ray. Therefore, we confirm, by careful analysis, that the transitions with energies of 384.0 and 537.2 keV are in coincidence with the 1695.0, 850.0, and 576.0 keV γ rays (shown in part A of Fig. 1), rather than the 1692.8, 678.0, and 570.7 keV γ rays. Besides, three new transitions with 133.5, 225.5, and 1779.5 keV are placed below the (12_1^+) state at 2818.1 keV.

In part D, three new transitions 607.5, 708.0, and 1878.0 keV are added to the level scheme. The doublet 607 keV transitions (with exact energies of 606.8 and 607.5 keV) are observed. The 607.5 keV transition has mutual coincidence with the 1878.0, 743.8, 597.5, 587.1, 584.5, and 282.0 keV transitions. And yet, the 607.5 and 1878.0 keV transitions are not in coincidence with the 933.0 and 2744.0 keV transitions. Thus, based on the coincidence relationship and the intensities, the 607.5 and 1878.0 keV transitions are placed between the $15^{(-)}$ level at 5556.7 keV and the (13_2^-) level at 3071.2 keV. The 708.0 keV transition is in coincidence with the 633.2, 1066.5, and 813.4 keV transitions, but not in coincidence with the 300.0 keV transition. Considering the coincidence relations and relative intensities of the 300.0 keV and 633.2 keV transitions, we reverse the order proposed in Ref. [35]. In the current work, the 1903.5 keV transition is indicated to be of $\Delta I = 2$ character, whereas in Ref. [34], it is described as an $M1$ transition. In addition, the 1903.5-keV transition is also observed in the previous study [35]. However its multipolarity and placement are incompatible with the reported results in Ref. [34]. Based on our measurements of multipolarity and energy summings, we confirm the multipolarity and placement of the 1903.5 keV transition as assigned in the current work, which are consistent with the assignments reported by Chakraborty, in Ref. [35].

III. SHELL-MODEL CALCULATIONS AND DISCUSSIONS

Most states of nuclei with $Z \approx 40$ and $N \approx 50$ were well elucidated within the $\pi(f_{5/2}, p_{3/2}, p_{1/2}, g_{9/2}) \otimes \nu(p_{1/2}, g_{9/2}, g_{7/2}, d_{5/2})$ shell model space [4–8,13–14,36,37]. The shell model calculations for the ^{90}Nb isotones ^{88}Y [38], ^{89}Zr [39], ^{91}Mo [39], ^{92}Tc [40], ^{93}Ru [39], and ^{94}Rh [14] reproduced a significant number of low and medium spins at relatively low excitation energy. These energy levels were well described by considering the protons and neutron holes in the $p_{1/2}$ and $g_{9/2}$ orbitals. The portrayals of the high spin levels are greatly improved by introducing neutron excitations across the $N = 50$ shell gap. To better illuminate the present level structure of ^{90}Nb , the shell-model calculation was carried out by considering proton and neutron core excitations across the ^{88}Sr core. The calculation was performed using the NUSHELLX code [41]. The GWB model space was utilized with the GW-BXG effective interaction. The single particle energies (SPEs) are derived from Refs. [5,7].

Figure 6 displays the comparison between the calculative energy levels and the experimental ones. The main configuration components were listed in Table II, where all the configurations are based on a single neutron hole in the $g_{9/2}$ orbital [except for the (16_7^+) level at 7035.8 keV]. For simplicity, we will discuss the protons in the $(f_{5/2}, p_{3/2}, p_{1/2}, g_{9/2})$ orbitals. At positive parity, the ground state of 8^+ and the state of 9^+ are considered as proton particle and neutron hole configuration where the remaining protons are paired up in combinations of the $f_{5/2}$, $p_{3/2}$, and $p_{1/2}$ orbitals. The (10_1^+) , (11_1^+) , (11_3^+) , (13_1^+) , (13_3^+) , (14_1^+) , and (15_2^+) states require the promotion of a proton pair from the $p_{1/2}$ orbital to the $g_{9/2}$ orbital with the $\pi(f_{5/2}^6 p_{3/2}^4 p_{1/2}^0 g_{9/2}^2)$ configurations contributing maximally. The 10_2^+ , (11_2^+) , (12_1^+) , (13_2^+) , and (14_2^+) states contain the $\pi(f_{5/2}^5 p_{3/2}^4 p_{1/2}^1 g_{9/2}^2)$ as the preponderant configuration, which corresponds to a proton from the $f_{5/2}$ orbital to move into the $p_{1/2}$ orbital. The energy levels ranging from about 4200 keV to 6700 keV [excluding (17_1^+) level at 5727.2 keV] are also dominated by the $\pi(f_{5/2}^5 p_{3/2}^4 p_{1/2}^1 g_{9/2}^2)$ configuration. Besides, the $\pi(f_{5/2}^5 p_{3/2}^3 p_{1/2}^2 g_{9/2}^2)$ configuration, which involves the protons from the $(f_{5/2}, p_{3/2})$ orbits across the $Z = 38$ subshell to the $p_{1/2}$ orbit, makes a small contribution to these energy levels. As the excitation energy and angular momentum increase, the (18_3^+) and $19^{(+)}$ states generate from the $\pi(f_{5/2}^4 p_{3/2}^4 p_{1/2}^0 g_{9/2}^5)$ configuration as the main component formed by promoting a proton pair in the $f_{5/2}$ orbit across $Z = 40$ subshell to the $g_{9/2}$ orbit. The observed (15_3^+) at 4421.2 keV level cannot be reproduced by the shell model calculation. The (15_3^+) state, near the (15_2^+) state in excitation energies, may be formed by another multiplet of the $\pi(g_{9/2}^3) \otimes \nu g_{9/2}^{-1}$ configuration of the (15_2^+) state. Additionally, the (15^+) at 4421.2 keV level in Ref. [34], is proposed as the $\pi(f_{5/2}^6 p_{3/2}^4 p_{1/2}^0 g_{9/2}^3)$ configuration based on the semiempirical shell-model calculations in ^{90}Nb . These results suggest that the (15_3^+) state can be predicted as the $\pi(f_{5/2}^6 p_{3/2}^4 p_{1/2}^0 g_{9/2}^3)$ configuration.

In addition, the new high energy transition with 2614.6 keV connects the (16_7^+) level at 7035.8 keV and the (15_3^+) level at 4421.2 keV. The striking common feature of the high energy transitions with $E_\gamma \approx 2.5$ MeV from the higher-spin levels is investigated in the neighboring $N = 49$ isotones by Arnell *et al.* [24]. In their work, these high-energy transitions are predicted as either promotion the protons from the $(f_{5/2}, p_{3/2})$ orbits over the $Z = 38$ subshell into the $(p_{1/2}, g_{9/2})$ orbits or one neutron from the $g_{9/2}$ orbit over the $N = 50$ shell closure into the $d_{5/2}$ orbit. The calculated (16_7^+) state corresponding to the configurations of the types $\pi(f_{5/2}^5 p_{3/2}^4 p_{1/2}^1 g_{9/2}^2) \otimes \nu g_{9/2}^{-2} d_{5/2}$, $\pi(f_{5/2}^4 p_{3/2}^4 p_{1/2}^2 g_{9/2}^3) \otimes \nu g_{9/2}^{-2} d_{5/2}$, and $\pi(f_{5/2}^6 p_{3/2}^4 p_{1/2}^0 g_{9/2}^3) \otimes \nu g_{9/2}^{-2} d_{5/2}$ suggests that the such high energy transition with 2614.6 keV at high spin level can be attributed to both the neutron excitations from the $g_{9/2}$ orbit across the $N = 50$ neutron shell and proton excitations from the $f_{5/2}$ orbit into the $p_{1/2}$ ($g_{9/2}$) orbit. The (16_6^+) level at 6514.4 keV, decaying to the (15_2^+) level at 4195.9 keV via 2318.5 keV transition, is generated by proton excitations over the energy gap for $Z = 40(38)$.

TABLE II. Major compositions of the configurations of states in ^{90}Nb . Each composition is formed with $p = [\pi(p(1), p(2), p(3), p(4)) \otimes \nu(n(1), n(2), n(3), n(4))]$, where $p(i)$ and $n(i)$ stand for the proton number in ($f_{5/2}, p_{3/2}, p_{1/2}, g_{9/2}$) orbits and neutron number in ($p_{1/2}, g_{9/2}, g_{7/2}, d_{5/2}$) orbits, respectively.

I^π (\hbar)	$E_{\text{(exp)}}$ (keV)	$E_{\text{(cal)}}$ (keV)	Configurations $\pi \otimes \nu$	components (%)	I^π (\hbar)	$E_{\text{(exp)}}$ (keV)	$E_{\text{(cal)}}$ (keV)	Configurations $\pi \otimes \nu$	components (%)
8 ⁺	0	0	6 4 0 3 \otimes 2 9 0 0	30.81	(16 ₄ ⁺)	5467.6 ^a			
			6 4 2 1 \otimes 2 9 0 0	16.49	(16 ₅ ⁺)	5759.6	6002	5 4 1 3 \otimes 2 9 0 0	41.34
			4 4 2 3 \otimes 2 9 0 0	15.26				5 3 2 3 \otimes 2 9 0 0	19.47
9 ⁺	813.4	773	6 4 0 3 \otimes 2 9 0 0	29.01				4 4 2 3 \otimes 2 9 0 0	14.27
			6 4 2 1 \otimes 2 9 0 0	15.12	(16 ₆ ⁺)	6514.4	6367	5 4 1 3 \otimes 2 9 0 0	25.23
			4 4 2 3 \otimes 2 9 0 0	10.58				5 3 2 3 \otimes 2 9 0 0	23.25
(10 ₁ ⁺)	946.9	1224	6 4 0 3 \otimes 2 9 0 0	28.38				6 3 1 3 \otimes 2 9 0 0	21.88
			5 4 1 3 \otimes 2 9 0 0	21.83	(16 ₇ ⁺)	7035.8	6887	5 4 1 3 \otimes 2 8 0 1	24.20
			4 4 2 3 \otimes 2 9 0 0	21.81				4 4 2 3 \otimes 2 8 0 1	22.18
10 ₂ ⁺	2063.1	2222	5 4 1 3 \otimes 2 9 0 0	63.04				6 4 0 3 \otimes 2 8 0 1	13.05
			6 4 0 3 \otimes 2 9 0 0	28.38	(17 ₁ ⁺)	5727.2	5988	5 4 1 3 \otimes 2 9 0 0	54.36
(11 ₁ ⁺)	2118.4	2015	6 4 0 3 \otimes 2 9 0 0	27.87				4 4 2 3 \otimes 2 9 0 0	14.79
			4 4 2 3 \otimes 2 9 0 0	20.87	(17 ₂ ⁺)	6284.3	6368	5 4 1 3 \otimes 2 9 0 0	38.87
			5 4 1 3 \otimes 2 9 0 0	20.37				5 3 2 3 \otimes 2 9 0 0	19.22
(11 ₂ ⁺)	2592.5	2349	5 4 1 3 \otimes 2 9 0 0	63.26				6 3 1 3 \otimes 2 9 0 0	19.10
(11 ₃ ⁺)	2689.3	2662	6 4 0 3 \otimes 2 9 0 0	30.17	17 ₃ ⁽⁺⁾	6741.3	6930	5 4 1 3 \otimes 2 9 0 0	44.42
			5 4 1 3 \otimes 2 9 0 0	26.38				6 3 1 3 \otimes 2 9 0 0	14.85
(12 ₁ ⁺)	2818.1	2943	5 4 1 3 \otimes 2 9 0 0	49.14				5 3 2 3 \otimes 2 9 0 0	12.63
			6 4 0 3 \otimes 2 9 0 0	13.72	(18 ₁ ⁺)	6422.4 ^a			
(13 ₁ ⁺)	3313.9	3015	6 4 0 3 \otimes 2 9 0 0	40.52	(18 ₂ ⁺)	6861.3 ^a			
			4 4 2 3 \otimes 2 9 0 0	18.35	18 ₃ ⁽⁺⁾	7485.1	7710	4 4 0 5 \otimes 2 9 0 0	50.75
(13 ₂ ⁺)	3496.1	3177	5 4 1 3 \otimes 2 9 0 0	74.53				5 3 0 5 \otimes 2 9 0 0	11.55
(13 ₃ ⁺)	3632.6	3505	6 4 0 3 \otimes 2 9 0 0	30.93				4 4 2 3 \otimes 2 9 0 0	11.36
			5 4 1 3 \otimes 2 9 0 0	20.58	19 ⁽⁺⁾	7767.1	7802	4 4 0 5 \otimes 2 9 0 0	50.48
(14 ₁ ⁺)	3753.4	3707	6 4 0 3 \otimes 2 9 0 0	38.07				4 4 2 3 \otimes 2 9 0 0	13.20
			5 4 1 3 \otimes 2 9 0 0	17.77				5 3 0 5 \otimes 2 9 0 0	10.66
			4 4 2 3 \otimes 2 9 0 0	17.57	9 ⁻	1809.7	1779	6 4 1 2 \otimes 2 9 0 0	35.50
(14 ₂ ⁺)	3974.2	3910	5 4 1 3 \otimes 2 9 0 0	60.83				5 4 2 2 \otimes 2 9 0 0	24.17
(14 ₃ ⁺)	4251.0	4125	5 4 1 3 \otimes 2 9 0 0	61.96				5 4 0 4 \otimes 2 9 0 0	11.95
			5 3 2 3 \otimes 2 9 0 0	18.07	11 ₁ ⁻	1879.9	2070	6 4 1 2 \otimes 2 9 0 0	71.07
(14 ₄ ⁺)	4336.1	4292	5 4 1 3 \otimes 2 9 0 0	71.77	(11 ₂ ⁻)	2257.5	2428	5 4 0 4 \otimes 2 9 0 0	44.29
			5 3 2 3 \otimes 2 9 0 0	12.65				5 4 2 2 \otimes 2 9 0 0	19.23
(14 ₅ ⁺)	4513.1	4656	6 3 1 3 \otimes 2 9 0 0	36.51	(12 ₁ ⁻)	2486.7	2703	6 4 1 2 \otimes 2 9 0 0	66.12
			5 3 2 3 \otimes 2 9 0 0	24.33				5 4 2 2 \otimes 2 9 0 0	10.65
(15 ₁ ⁺)	4066.8	3868	5 4 1 3 \otimes 2 9 0 0	77.19	(13 ₁ ⁻)	2812.9	2831	5 4 0 4 \otimes 2 9 0 0	47.14
(15 ₂ ⁺)	4195.9	4217	6 4 0 3 \otimes 2 9 0 0	46.66				5 4 2 2 \otimes 2 9 0 0	20.47
			4 4 2 3 \otimes 2 9 0 0	15.38	(13 ₂ ⁻)	3071.2	3310	6 4 1 2 \otimes 2 9 0 0	69.71
(15 ₃ ⁺)	4421.2 ^a				13 ₃ ⁻	3653.9	3863	5 4 0 4 \otimes 2 9 0 0	37.11
(15 ₄ ⁺)	4537.4	4878	5 4 1 3 \otimes 2 9 0 0	52.42				5 3 1 4 \otimes 2 9 0 0	18.64
			4 4 2 3 \otimes 2 9 0 0	12.90	(14 ₁ ⁻)	3678.7	3661	5 4 0 4 \otimes 2 9 0 0	45.68
			5 3 2 3 \otimes 2 9 0 0	10.56				4 4 1 4 \otimes 2 9 0 0	16.43
(15 ₅ ⁺)	4897.1	5005	5 4 1 3 \otimes 2 9 0 0	67.78				5 4 2 2 \otimes 2 9 0 0	11.18
			5 3 2 3 \otimes 2 9 0 0	16.31	(14 ₂ ⁻)	4329.4	4711	5 4 0 4 \otimes 2 9 0 0	24.46
(15 ₆ ⁺)	5150.4	5385	5 4 1 3 \otimes 2 9 0 0	47.22				5 4 2 2 \otimes 2 9 0 0	19.75
			5 3 2 3 \otimes 2 9 0 0	11.83				4 4 1 4 \otimes 2 9 0 0	19.01
(16 ₁ ⁺)	5029.4	4730	5 4 1 3 \otimes 2 9 0 0	71.18	15 ⁽⁻⁾	5556.7	5555	5 4 2 2 \otimes 2 9 0 0	32.20
			5 3 2 3 \otimes 2 9 0 0	14.32				4 4 1 4 \otimes 2 9 0 0	20.26
(16 ₂ ⁺)	5380.2	5493	5 4 1 3 \otimes 2 9 0 0	62.91				5 3 1 4 \otimes 2 9 0 0	12.29
			5 3 2 3 \otimes 2 9 0 0	18.31	16 ⁽⁻⁾	6154.2	6059	5 3 1 4 \otimes 2 9 0 0	40.18
(16 ₃ ⁺)	5434.3	5616	5 4 1 3 \otimes 2 9 0 0	68.31				4 4 1 4 \otimes 2 9 0 0	19.21
			5 3 2 3 \otimes 2 9 0 0	8.02				6 3 1 3 \otimes 2 9 0 0	21.88

^aShell model calculation fails to reproduce these levels.

The main configurations of the 9^- state contain the $\pi(f_{5/2}^6 p_{3/2}^4 p_{1/2}^2 g_{9/2}^2)$ and $\pi(f_{5/2}^5 p_{3/2}^4 p_{1/2}^2 g_{9/2}^2)$. The 11^- , (12^-) , and 13^- states are dominated by $\pi(f_{5/2}^6 p_{3/2}^4 p_{1/2}^2 g_{9/2}^2)$ configuration. This configuration comes from moving the odd proton from the $g_{9/2}$ orbital to the $p_{1/2}$ orbital. The (11^-) , (13^-) , 13^- , (14^-) , and (14^-) states are formed by the configuration of the $\pi(f_{5/2}^5 p_{3/2}^4 p_{1/2}^2 g_{9/2}^2)$, which results from breaking a proton pair in the $f_{5/2}$ orbit and exciting one proton to the $g_{9/2}$ orbit. The $15^{(-)}$ level at 5556.7 keV, decaying to the (13^-) level at 2812.9 keV by a high energy transition (2774.0 keV), corresponds to the $\pi(f_{5/2}^5 p_{3/2}^4 p_{1/2}^2 g_{9/2}^2)$ configuration, resulting from breaking a proton pair in the $f_{5/2}$ orbit to the $p_{1/2}$ orbit and admixtures of the $\pi(f_{5/2}^4 p_{3/2}^4 p_{1/2}^2 g_{9/2}^2)$ configuration, where a proton is moved from the $f_{5/2}$ orbit to the $g_{9/2}$ orbit and with the odd proton in the $p_{1/2}$ orbital. Similar features were also reported in its neighboring nuclei, ^{90}Zr and ^{91}Nb at medium-spin levels [5,6]. In ^{90}Zr , the high energy (2688.7 keV) transition connects the 11^+ level at 6277.1 keV and the (8_1^+) level at 3588.4 keV. In ^{91}Nb , the $(21/2^-)$ level at 6027.9 keV and $(21/2^-)$ level at 5956.7 keV decay to the $21/2_1^+$ level at 3465.6 keV by the high energy transitions with 2562.0 and 2490.8 keV, respectively. From the shell model calculations, these high energy transitions are reported to have the similar configurations, i.e., the promotion of protons from the $(f_{5/2}, p_{3/2})$ orbitals across the $Z = 38$ subshell to the $(p_{1/2}, g_{9/2})$ orbitals. The main configuration of the $16^{(-)}$ state is proposed as the $\pi(f_{5/2}^5 p_{3/2}^3 p_{1/2}^2 g_{9/2}^2)$, which stems from the breakup of the $f_{5/2}$ and $p_{3/2}$ pairs with the two protons creating an additional $g_{9/2}$ pair and placing the odd proton in the $p_{1/2}$ orbital.

IV. SYSTEMATICS OF LEVEL STRUCTURE CHARACTERISTICS NEAR $A = 90$

Figure 7 demonstrates the level sequences in ^{90}Nb and its neighboring isotopes. From ^{85}Nb to ^{91}Nb [42–48], the excitation energies of the 10^+ and 12^+ states in ^{90}Nb are significantly larger than those of ^{88}Nb and ^{86}Nb as well as the $13/2^+$ and $17/2^+$ states in ^{87}Nb and ^{89}Nb , while close to those of ^{91}Nb . As the neutron number increases, the level structures tend to become more similar. The level sequences demonstrate the obvious collective structures with a regular rotational dependence of $E \propto I(I+1)$ for the lighter Nb isotopes (^{85}Nb , ^{87}Nb , ^{88}Nb , and ^{89}Nb). However, for the heavier nuclei ^{90}Nb and ^{91}Nb , the irregular spacings of the energy levels indicate the presence of single-particle nature even at high spins and excitation energies. An efficacious way to differentiate between the spherical and collective characteristics is by extracting the ratios of the two lowest-level energies relative to the ground states from experiments. As examples [see Fig. 7(c)], the energy ratios $R = (E_{17/2^+} - E_{9/2^+}) / (E_{13/2^+} - E_{9/2^+})$ for ^{86}Nb and $R = (E_{12^+} - E_{8^+}) / (E_{10^+} - E_{8^+})$ for ^{87}Nb are about 2.2, which manifest collective behavior with moderate deformations. For ^{88}Nb and ^{89}Nb , the energy ratios R of about 1.9 may indicate either vibrational collectivity or a balanced mixture of single-particle and collective behaviors. The energy ratios R for that in ^{90}Nb and ^{91}Nb are about 1.3, which show single-particle behavior of the yrast spectra of ^{90}Nb and ^{91}Nb , and can be explained by intrinsic excitation.

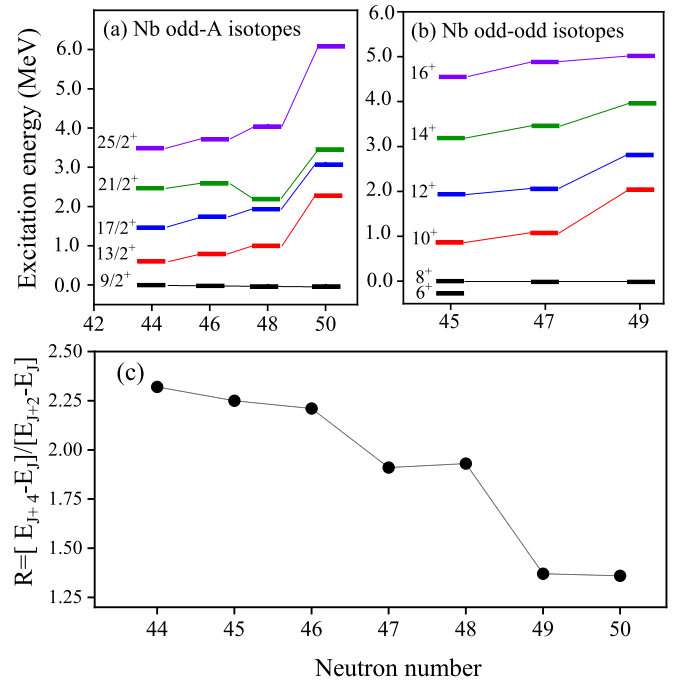


FIG. 7. (a) The level energies in Nb odd-A isotopes; (b) the same as (a), but for Nb odd-odd isotopes; (c) the ratios of the two lowest level energies observed relative to ground states. $R = [E_{I+4} - E_I] / [E_{I+2} - E_I]$, with $I = 9/2$ for odd-A nuclei and $I = 8$ for odd-odd nuclei.

To investigate more information about the correlation between level structure in ^{90}Nb and its neighboring nuclei, the energies of the levels in ^{88}Nb [15], ^{89}Nb [49], ^{91}Nb [6], ^{90}Tc [17], ^{91}Tc [50], ^{92}Tc [40], and ^{93}Tc [12] are shown in Fig. 8.

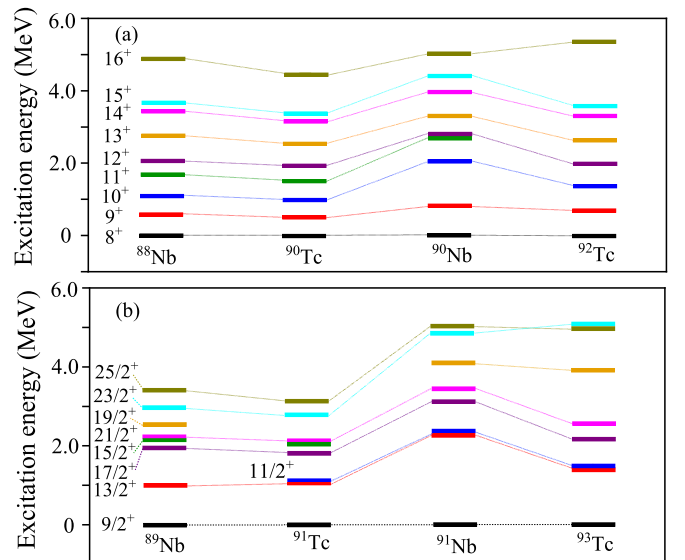


FIG. 8. (a) Comparison between the energy levels up to the $16^+ \hbar$ in ^{90}Nb and its odd-odd neighbors nuclei ^{88}Nb , ^{90}Tc and ^{92}Tc ; (b) Comparison between the energy levels up to the $25/2^+ \hbar$ in ^{89}Nb and its odd-A neighbors nuclei ^{91}Nb , ^{91}Tc , and ^{93}Tc .

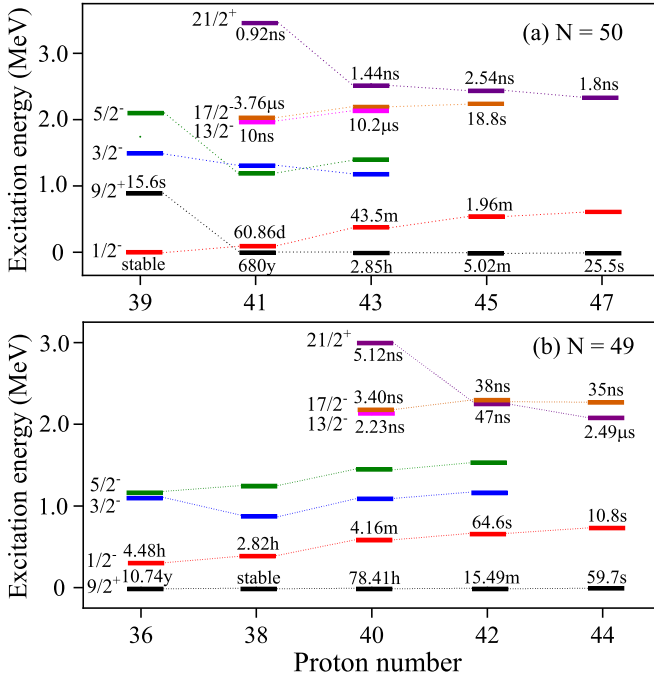


FIG. 9. (a) Energy levels and isomer half-lives in the $N = 50$ isotones; (b) the same as (a), but for $N = 49$ isotones.

There is an obvious similarity between the level structure in ^{88}Nb (^{89}Nb) and ^{90}Tc (^{91}Tc), which may be interpreted by postulating that adding or subtracting pairs of nucleons in ^{88}Nb and ^{90}Tc has only a little impact on the excitation pattern. Whilst the energies of the levels in ^{90}Nb and ^{92}Tc are significantly higher than those in ^{88}Nb and ^{90}Tc up to the $12^+\hbar$. The 10^+ and 12^+ states in ^{88}Nb and ^{90}Tc are interpreted as $\pi(g_{9/2}) \otimes \nu(g_{9/2}^{-3})$ and $\pi(g_{9/2}) \otimes \nu(g_{9/2}^{-3})$ multiplets, respectively. As the neutron number increases, ^{92}Tc and ^{90}Nb possess only one neutron hole with respect to the $N = 50$ shell closure. Thus the breakup a $g_{9/2}$ proton pair may be used to increase spin. In addition, the excitation energies of the $I = 13/2^+$ to $25/2^+$ states in ^{91}Nb and ^{93}Tc are apparently greater than those in ^{89}Nb and ^{91}Tc . This may be due to the absence of valence-neutron holes in the $g_{9/2}$ orbit in ^{91}Nb and ^{93}Tc . The level schemes of ^{88}Nb and ^{90}Tc exhibit a greater similarity compared to those of ^{90}Nb and ^{92}Tc . That is, the addition of one more neutron enables the level structures in ^{90}Nb and ^{92}Tc to become more complex and less regular than those in ^{88}Nb and ^{90}Tc .

Figure 9(a) shows the evolutionary trends of the first $9/2^+$, $1/2^-$, $3/2^-$, and $5/2^-$ levels in the $N = 50$ isotones with even-numbered protons [46,48,51–53]. The $3/2^-$ and $5/2^-$ levels correspond to the $p_{3/2}$ and $f_{5/2}$ single proton hole states in ^{89}Y , ^{91}Nb and ^{92}Tc , and the $9/2^+$ and $1/2^-$ states correspond to the $g_{9/2}$ and $p_{1/2}$ single particle states in ^{89}Y , ^{91}Nb , ^{93}Tc , ^{95}Rh [52] and ^{97}Ag [53]. The energies of the first $1/2^-$ states increase gradually along with the number of protons, indicating that the energy gap between the $g_{9/2}$ and $p_{1/2}$ orbits increases gradually as the proton number increases. Moving to the $N = 49$ isotones, the characteristic of one neutron hole states corresponding to the $N = 50$ neutron shell can

provide pertinent and valuable information on nucleon-nucleon effective interactions and nucleon-nucleon correlations in the shell-model framework. We therefore focus on the energy levels of the neutron hole states for the $N = 49$ isotones with even-numbered protons [46,48,51,54,55] [shown in Fig. 9(b)]. Figure 9(b) displays that the energies of the $1/2^-$, $3/2^-$, and $5/2^-$ single neutron hole states change smoothly with $Z = 38$ – 42 . The energies of these neutron hole states are in accord with the order of the $p_{1/2}$, $p_{3/2}$, and $f_{5/2}$ orbits, which is different from that of the proton hole states in the $N = 50$ nuclei. In addition, it is interesting to note that odd-odd nuclei ^{89}Y , ^{91}Nb , ^{93}Tc , and ^{95}Rh ($N = 50$) exhibit an $M4$ isomeric transition, depopulating a proton-hole excited state. Along the $N = 49$ isotone chain, the $1/2^-$ isomers are a common and unifying feature of the odd- A nuclei ranging from ^{85}Kr up to ^{93}Ru . Case in point, the $1/2^-$ isomer at 587.8 keV with a half-life of 4.16 min in ^{89}Zr is explained as a single-particle $\nu p_{1/2}$ configuration [40]. Another feature observed along the $N = 49$ (50) isotones is the presence of shorter-lived isomers above the $1/2^-$ states, e.g., the $21/2^+$ isomers in ^{89}Zr , ^{91}Mo , and ^{93}Ru were reported at 2995.3, 2267.4, and 2082.5 keV, respectively with half-lives of 5.12 ns [46], 38 ns [48], and 2.49 μs [51]. The results may indicate that the isomeric states in the odd- A nuclei are interpreted as the extra binding energy originating from the large attractive proton-neutron interaction in the maximally aligned particle or hole configurations.

V. SUMMARY

Excited levels in the level structure of the ^{90}Nb nucleus were investigated through the reaction $^{76}\text{Ge}(^{19}\text{F}, 5n)^{90}\text{Nb}$. Twenty-eight new transitions and 25 levels were located in the level scheme of the ^{90}Nb nucleus. The newly established level structure was investigated by the shell model calculations with the $\pi(f_{5/2}, p_{3/2}, p_{1/2}, g_{9/2}) \otimes \nu(p_{1/2}, g_{9/2}, d_{5/2})$ model space, which clearly stated that most of the positive parity states and the negative parity states up to the maximum spin observed in the current experiment can be well described by the valence proton states in the fpg orbits coupled with a single neutron hole in the $g_{9/2}$ orbital. Only the (16_7^+) level at 7035.8 keV was interpreted as neutron excitations from the $g_{9/2}$ orbit across the $N = 50$ shell closure into the $d_{5/2}$ orbit coupled with proton excitations from the $f_{5/2}$ orbit into the $p_{1/2}$ ($g_{9/2}$) orbit. Additionally, the investigation of single neutron hole states in the $N = 49$ isotones and proton hole states in the $N = 50$ isotones enlightens that the high-spin isomers in the nuclei around the shell closure are formed when the neutron number and/or proton number outside the closed shell is an odd number.

ACKNOWLEDGMENTS

The authors gratefully acknowledge all the HI-13 tandem accelerator staff and Dr. Q. W. Fan for assistance during the preparation of target. This work is supported by the National Natural Science Foundation of China under Grant No. U1867210 and Key Program of the Education Department of Anhui Province under Grants No. KJ2017A365, No. 2023AH050481, and No. 2023AH050514.

- [1] M. Bunce, P. H. Regan, V. Werner, C. W. Beausang, V. Anagnostatou, M. Bowry, R. J. Casperson, D. Chen, N. Cooper, P. M. Goddard, R. O. Hughes, G. Ilie, P. J. R. Mason, B. Pauerstein, M. W. Reed, T. J. Ross, and E. C. Simpson, *Phys. Rev. C* **87**, 044337 (2013).
- [2] F. H. Al-Khudair and M. M. Mahdi, *Phys. Rev. C* **108**, 014305 (2023).
- [3] Z. Huang, G. X. Zhang, C. X. Yuan, G. L. Zhang, D. Mengoni, B. S. Cai, S. P. Hu, H. Q. Zhang, H. B. Sun, J. J. Valiente-Dobón, D. Testov, A. Goasduff, D. Bazzacco, D. R. Napoli, F. Galtarossa, F. Recchia, G. de Angelis, M. Siciliano, R. Menegazzo, and S. M. Lenzi, *Phys. Rev. C* **107**, 044309 (2023).
- [4] Z. Huang, G. X. Zhang, G. L. Zhang, S. P. Hu, S. M. Lenzi, D. Mengoni, J. L. Ferreira, Y. F. Lv, J. B. Lu, B. Paes, E. N. Cardozo, H. Q. Zhang, H. B. Sun, J. J. Valiente-Dobón, D. Testov, A. Goasduff, D. Bazzacco, P. R. John, D. R. Napoli, F. Galtarossa *et al.*, *Phys. Rev. C* **106**, 064331 (2022).
- [5] P. Dey, D. Negi, R. Palit, P. C. Srivastava, Md. S. R. Laskar, B. Das, F. S. Babra, S. Bhattacharya, Biswajit Das, K. Rojeeta Devi, R. Gala, U. Garg, S. S. Ghugre, E. Ideguchi, S. Kumar, A. Kundu, G. Mukherjee, S. Muralithar, S. Nag, S. Nandi, Neelam, M. Kumar Raja, R. Raut *et al.*, *Phys. Rev. C* **105**, 044307 (2022).
- [6] Y. H. Wu, J. B. Lu, Z. Ren, T. J. Gao, P. Y. Yang, Y. Hao, G. J. Fu, J. Li, K. Y. Ma, X. G. Wu, Y. Zheng, and C. B. Li, *Phys. Rev. C* **106**, 054326 (2022).
- [7] P. W. Luo, X. G. Wu, H. B. Sun, G. S. Li, C. Y. He, Y. Zheng, C. B. Li, S. P. Hu, Y. H. Wu, H. W. Li, J. J. Liu, J. L. Wang, S. H. Yao, and S. A. Edwards, *Phys. Rev. C* **89**, 034318 (2014).
- [8] Y. Zheng, Y. H. Wu, X. G. Wu, C. B. Li, L. H. Zhu, T. X. Li, P. W. Luo, G. S. Li, C. Y. He, H. W. Li, S. P. Hu, J. J. Liu, J. L. Wang, S. H. Yao, Q. M. Chen, J. Zhong, J. B. Lu, K. Y. Ma, and D. Yang, *Phys. Rev. C* **100**, 014325 (2019).
- [9] B. A. Brown, P. M. S. Lesser, and D. B. Fossan, *Phys. Rev. C* **13**, 1900 (1976).
- [10] P. Singh, R. G. Pillay, J. A. Sheikh, and H. G. Devare, *Phys. Rev. C* **45**, 2161 (1992).
- [11] R. Schwengner, R. Massarczyk, G. Rusev, N. Tsoneva, D. Bemmerer, R. Beyers, R. Hannaske, A. R. Junghans, J. H. Kelley, E. Kwan, H. Lenske, M. Marta, R. Raut, K. D. Schilling, A. Tonchev, W. Tornow, and A. Wagner, *Phys. Rev. C* **87**, 024306 (2013).
- [12] M. Hausmann, A. Jungclaus, E. Galindo, K. P. Lieb, O. Yordanov, I. P. Johnstone, R. Schwengner, A. Dewald, A. Fitzler, O. Möller, G. de Angelis, A. Gadea, T. Martinez, D. R. Napoli, and C. Ur, *Phys. Rev. C* **68**, 024309 (2003).
- [13] F. Ghazi Moradi, C. Qi, B. Cederwall, A. Ataç, T. Bäck, R. Liotta, M. Doncel, A. Johnson, G. de France, E. Clément, A. Dijon, R. Wadsworth, T. W. Henry, A. J. Nichols, H. Al-Azri, J. Nyberg, A. Gengelbach, T. Hüyük, B. M. Nyakó, J. Timár, D. Sohler, Zs. Dombrádi, I. Kuti *et al.*, *Phys. Rev. C* **89**, 014301 (2014).
- [14] H. A. Roth, S. E. Arnell, D. Foltescu, Ö. Skeppstedt, J. Blomqvist, A. Nilsson, T. Kuroyanagi, S. Mitarai, and J. Nyberg, *Phys. Rev. C* **50**, 1330 (1994).
- [15] R. Schubart, A. Jungclaus, A. Harder, M. K. Kabadiyski, K. P. Lieb, D. Rudolph, M. Weiszflog, S. Albers, T. Burkardt, J. Eberth, M. Eschenauer, M. Luig, N. Nicolay, and H. Grawe, *Nucl. Phys. A* **591**, 515 (1995).
- [16] G. García-Bermúdez, M. A. Cardona, R. V. Ribas, A. Filevich, E. Achterberg, and L. Szybisz, *Phys. Rev. C* **48**, 1623 (1993).
- [17] D. Rudolph, C. J. Gross, M. K. Kabadiyski, K. P. Lieb, M. Weiszflog, H. Grawe, J. Heese, K. H. Maier, and J. Eberth, *Phys. Rev. C* **47**, 2574 (1993).
- [18] Y. Zheng, G. de France, E. Clément, A. Dijon, B. Cederwall, R. Wadsworth, T. Bäck, F. Ghazi Moradi, G. Jaworski, B. M. Nyakó, J. Nyberg, M. Palacz, H. Al-Azri, G. de Angelis, A. Ataç, Ö. Aktaş, S. Bhattacharyya, T. Brock, P. J. Davies, 4 A. Di Nitto, Zs. Dombrádi, A. Gadea, J. Gál, P. Joshi *et al.*, *Phys. Rev. C* **87**, 044328 (2013).
- [19] M. K. Kabadiyski, C. J. Gross, A. Harder, K. P. Lieb, D. Rudolph, M. Weiszflog, J. Altmann, A. Dewald, J. Eberth, T. Mylaeus, H. Grawe, J. Heese, and K. H. Maier, *Phys. Rev. C* **50**, 110 (1994).
- [20] K. Lagergren, B. Cederwall, R. M. Clark, P. Fallon, A. Görgen, T. Issa, R. V. F. Janssens, A. Johnson, A. O. Macchiavelli, L. Milechina, D. G. Sarantites, and R. Wyss, *Phys. Rev. C* **68**, 064309 (2003).
- [21] D. Bucurescu, N. Mărginean, C. Rossi Alvarez, Y. Sun, C. A. Ur, L. C. Mihăilescu, G. Suliman, D. Bazzacco, S. Lunardi, G. de Angelis, M. Axiotis, E. Farnea, A. Gadea, M. Ionescu-Bujor, A. Iordăchescu, W. Krolas, Th. Kröll, S. M. Lenzi, T. Martinez, R. Menegazzo, D. R. Napoli, P. Pavan, Zs. Podolyak *et al.*, *Phys. Rev. C* **69**, 064319 (2004).
- [22] M. Wiedeking, S. L. Tabor, F. Cristancho, M. Devlin, J. Döring, C. B. Jackson, G. D. Johns, R. A. Kaye, I. Y. Lee, F. Lerma, A. O. Macchiavelli, M. Naidu, I. Ragnarsson, D. G. Sarantites, and G. Z. Solomon, *Phys. Rev. C* **67**, 034320 (2003).
- [23] J. Pavan, S. L. Tabor, A. V. Afanasjev, C. Baktash, F. Cristancho, M. Devlin, J. Döring, C. J. Gross, G. D. Johns, R. A. Kaye, D. R. LaFosse, I. Y. Lee, F. Lerma, A. O. Macchiavelli, I. Ragnarsson, D. G. Sarantites, and G. N. Solomon, *Phys. Rev. C* **85**, 044322 (2012).
- [24] S. E. Arnell, D. Foltescu, H. A. Roth, Ö. Skeppstedt, J. Blomqvist, A. Nilsson, T. Kuroyanagi, S. Mitarai, and J. Nyberg, *Phys. Rev. C* **49**, 51 (1994).
- [25] S. Saha, R. Palit, J. Sethi, T. Trivedi, P. C. Srivastava, S. Kumar, B. S. Naidu, R. Donthi, S. Jadhav, D. C. Biswas, U. Garg, A. Goswami, H. C. Jain, P. K. Joshi, G. Mukherjee, Z. Naik, S. Nag, V. Nanal, R. G. Pillay, S. Saha *et al.*, *Phys. Rev. C* **86**, 034315 (2012).
- [26] S. Ray, N. S. Pattabiraman, R. Goswami, S. S. Ghugre, A. K. Sinha, and U. Garg, *Phys. Rev. C* **69**, 054314 (2004).
- [27] Z. Ren, J. B. Lu, G. L. Zhang, Y. H. Wu, T. J. Gao, K. Y. Ma, Z. Huang, G. X. Zhang, M. L. Wang, S. P. Hu, H. B. Sun, H. Q. Zhang, D. Testov, P. R. John, J. J. Valiente-Dobon, A. Goasduff, M. Siciliano, F. Galtarossa, D. Mengoni, and D. Bazzacco, *Phys. Rev. C* **106**, 024323 (2022).
- [28] P. Singh, R. G. Pillay, J. A. Sheikh, and H. G. Devare, *Phys. Rev. C* **48**, 1609 (1993).
- [29] E. K. Warburton, J. W. Olness, C. J. Lister, R. W. Zurmühle, and J. A. Becker, *Phys. Rev. C* **31**, 1184 (1985).
- [30] R. Schwengner, J. Reif, H. Schnare, G. Winter, T. Servene, L. Käubler, H. Prade, M. Wilhelm, A. Fitzler, S. Kasemann, E. Radermacher, and P. von Brentano, *Phys. Rev. C* **57**, 2892 (1998).
- [31] J. A. Cooper, J. M. Hollander and J. O. Rasmussen, *Nucl. Phys. A* **109**, 603 (1967).
- [32] D. E. Bainum, J. Rapaport, C. D. Goodman, D. J. Horen, C. C. Foster, M. B. Greenfield, and C. A. Goulding, *Phys. Rev. Lett.* **44**, 1751 (1980).

- [33] C. A. Fields, F. W. N. De Boer, J. J. Kraushaar, R. A. Ristinen, L. E. Samuelson, and E. Sugarbaker, *Nucl. Phys. A* **363**, 311 (1981).
- [34] X. Z. Cui, L. H. Zhu, X. G. Wu, Z. M. Wang, C. Y. He, Y. Liu, G. S. Li, S. X. Wen, Z. L. Zhang, R. Meng, R. G. Ma, P. Luo, Y. Zheng, M. M. Ndontchueng, J. D. Huo, and C. X. Yang, *Phys. Rev. C* **72**, 044322 (2005).
- [35] A. Chakraborty, Krishichayan, S. S. Ghugre, R. Goswami, S. Mukhopadhyay, N. S. Pattabiraman, S. Ray, A. K. Sinha, S. Sarkar, P. V. Madhusudhana Rao, U. Garg, S. K. Basu, M. B. Chatterjee, M. S. Sarkar, L. Chaturvedi, A. Dhal, R. K. Sinha, I. M. Govil, R. K. Bhowmik, A. Jhingan, N. Madhavan, S. Muralithar *et al.*, *Phys. Rev. C* **72**, 054309 (2005).
- [36] M. Palacz, J. Nyberg, H. Grawe, K. Sieja, G. de Angelis, P. Bednarczyk, A. Blazhev, D. Curien, Z. Dombradi, O. Dorvaux, J. Ekman, J. Ga lkowski, M. Górska, J. Iwanicki, G. Jaworski, J. Kownacki, J. Ljungvall, M. Moszyński, F. Nowacki, D. Rudolph, D. Sohler, D. Wolski, and M. Ziębliński, *Phys. Rev. C* **96**, 014318 (2012).
- [37] N. S. Pattabiraman, S. N. Chintalapudi, S. S. Ghugre, B. V. Tirumala Rao, M. L. N. Raju, T. S. Reddy, P. K. Joshi, R. Palit, and H. C. Jain, *Phys. Rev. C* **65**, 044324 (2002).
- [38] H. W. Baer, R. L. Bunting, J. E. Glenn, and J. J. Kraushaar, *Nucl. Phys. A* **218**, 355 (1974).
- [39] A. Nilsson and M. Grecescu, *Nucl. Phys. A* **212**, 448 (1973).
- [40] C. A. Fields, F. W. N. de Boer, and B. J. Diana, *Nucl. Phys. A* **401**, 117 (1983).
- [41] B. Brown and W. Rae, *Nucl. Data Sheets* **120**, 115 (2014).
- [42] K. Jonsson, B. Cederwall, A. Johnson, R. Wyss, T. Bäck, J. Cederkäll, M. Devlin, J. Elson, D. R. LaFosse, F. Lerma, D. G. Sarantites, R. M. Clark, I. Y. Lee, A. O. Macchiavelli, and R. W. Macleod, *Nucl. Phys. A* **645**, 47 (1999).
- [43] A. Negret and B. Singh, *Nucl. Data Sheets* **124**, 1 (2015).
- [44] C. Teich, A. Jungclaus, V. Fischer, D. Kast, K. P. Lieb, C. Lingk, C. Ender, T. Härtlein, F. Köck, D. Schwalm, J. Billowes, J. Eberth, and H. G. Thomas, *Phys. Rev. C* **59**, 1943 (1999).
- [45] E. A. McCutchan and A. A. Sonzogni, *Nucl. Data Sheets* **115**, 135 (2014).
- [46] B. Singh, *Nucl. Data Sheets* **114**, 1 (2013).
- [47] E. Browne, *Nucl. Data Sheets* **82**, 379 (1997).
- [48] C. M. Baglin, *Nucl. Data Sheets* **114**, 1293 (2013).
- [49] P. Singh, R. Palit, S. Saha, J. Sethi, S. Biswas, D. Choudhury, P. C. Srivastava, and T. Trivedi, *Phys. Rev. C* **90**, 014306 (2014).
- [50] D. Rudolph, C. J. Gross, A. Harder, M. K. Kabadiyski, K. P. Lieb, M. Weiszflog, J. Altmann, A. Dewald, J. Eberth, T. Mylaeus, H. Grawe, J. Heese, and K.-H. Maier, *Phys. Rev. C* **49**, 66 (1994).
- [51] C. M. Baglin, *Nucl. Data Sheets* **112**, 1163 (2011).
- [52] S. K. Basu and G. Mukherjee, *Nucl. Data Sheets* **111**, 2555 (2010).
- [53] N. Nica, *Nucl. Data Sheets* **111**, 525 (2010).
- [54] B. Singh and J. Chen, *Nucl. Data Sheets* **116**, 1 (2014).
- [55] T. D. Johnson and W. D. Kulp, *Nucl. Data Sheets* **129**, 1 (2015).